Proceedings of 2013 ASME Pressure Vessels and Piping Division Conference
PVP2013
July 14-18, 2013, Paris, France

PVP2013-97115

RESPONSE OF PIPING TEES TO PROPAGATING DETONATIONS

Thomas C. Ligon and David J. Gross
Dominion Engineering, Inc.
Reston, Virginia, USA

Joseph E. Shepherd
Graduate Aerospace Laboratories
California Institute of Technology
Pasadena, California, USA

ABSTRACT

This paper reports the results of experiments and finite element simulations on the structural response of piping systems to internal detonation loading. Specifically, the work described in this paper focuses on the forces that are produced at tee-junctions that lead to axial and bending structural responses of the piping system.

Detonation experiments were conducted in a 2-in. (50 mm) diameter schedule 40 piping system that was fabricated using 304 stainless steel and welded to ASME B31.3 standards. The 4.1 m (162-in.) long piping system included one tee and was supported using custom brackets and cantilever beams fastened to steel plates that were bolted to the laboratory walls. Nearly-ideal detonations were used in a 30/70 H_2-N_2O mixture at 1 atm initial pressure and 300 K. Pressure and hoop, axial, and support strains were measured using a high-speed (1 MHz) digital data acquisition system and calibrated signal conditioners.

It was concluded that detonations propagate through the run of a 90º tee with relatively little disturbance in either direction. The detonation load increases by approximately a factor of 2 when the detonation enters through the branch. The deflections of the cantilever beam supports and the hoop and axial pipe strains could be adequately predicted by finite element simulations. The support loads are adequately predicted as long as the supports are constrained to the piping.

This paper shows that with relatively simple models, quantitative predictions of tee forces can be made for the purposes of design or safety analysis of piping systems subject to internal detonations.

NOMENCLATURE

A	Pipe Cross-Sectional Area
c_0	Longitudinal Sound Velocity
c_{CJ}	Sound Velocity at the CJ State
c_3	Post-Expansion Region Sound Velocity
CJ	Chapman-Jouguet
DLF	Dynamic Load Factor
E	Modulus of Elasticity
γ_2	Detonation Products Ratio of Specific Heats
P_{CJ}	CJ Detonation Pressure
P_3	Post-Expansion Region Pressure
P_{det}	TZ Detonation Pressure Time-History
ρ	Density
v	Poisson's Ratio
t	Time
TZ	Taylor-Zel'dovich
u	Velocity
U_{CJ}	CJ Detonation Velocity
R	Pipe Mid-Radius
x	Axial distance along the pipe

INTRODUCTION

The potential for explosion hazards in piping at the Hanford Tank Waste Treatment and Immobilization Plant (WTP) has motivated the study of structural response of piping systems to gaseous detonations. Flammable gases may build up within the piping system and ignition may result in a propagating flame that may, under certain conditions, transition to a detonation [1],[2]. The detonation pressure load excites a wide spectrum of mechanical vibration modes in a piping system [3],[4]. If a piping system is to be analyzed to withstand a detonation, all of the response modes must be considered in the analysis. In addition, the interactions between the detonation and piping system components must be understood.

A detonation propagating within a pipe represents a traveling load in the form of a step or jump in pressure followed by an expansion wave. Ideal detonations propagate at approximately the Chapman-Jouguet (CJ) detonation speed and the detonation pressure axisymmetrically loads the pipe. The structural response of a straight pipe to a detonation propagating at a constant speed was studied in depth by Beltman [5], but industrial piping systems are more complex.

 See Note 1 under Acknowledgements

Unlike straight pipe, piping systems include components such as bends, tees, and closed-ends that perturb the detonation. These perturbations generally cause the detonation loads to increase. Recent investigations [4],[6] have studied the response at closed-ends and piping bends. In both cases, the details of how the components perturb the detonation have a significant impact on the resulting structural response.

The focus of this paper is on piping tees. Detonations may enter a tee through either the branch or the run. The primary objective is to establish pressure time-history models that appropriately represent the loads that are developed in the tee. Intuition suggests that the forces associated with a detonation entering though the run or branch would differ significantly. When the detonation enters through the branch, the momentum of the explosion products behind the detonation front are turned in the direction of the run. Conversely, the momentum behind a detonation entering through the run can continue through the tee without significant perturbation.

A simple piping system with one tee, designated *TS-1*, was built to support this study. The system was filled with a mixture of hydrogen and nitrous oxide gas and ignited at two different ends of the system. These experiments produced detonations that propagated through the run and branch of the tee. These experiments produced strain measurements of the resulting pipe and support response. The detonation pressure models were validated by comparing strain results from finite-element simulations to the measured strain data.

Experimental Apparatus and Description

The test apparatus was a 2-in. schedule 40 piping system constructed from ASTM A312 type 304 stainless steel with a nominal 3.8 mm (0.154 in.) wall thickness [7]. The piping system included a single tee that was butt welded to an approximately 1.5 m long vertical section and two approximately 1.2 m long horizontal sections (see Figure 1). Class 300 lb slip-on flanges were welded to the three ends of the pipe. All welding was certified to ASME B31.3 standards.

The system was supported on short (17.8 cm long) steel cantilever beams, to allow measurement of the reaction loads. The cross-section of the cantilever was a 25.4 mm (1 in.) by 31.8 mm (1.25 in.) rectangle with the longer side perpendicular to the axis of the pipe. The pipe was connected to the beams using standard u-bolts. Two cantilever beams were located 76 mm from the two blind flanges on the horizontal run, and their u-bolts were clamped down on the pipe to restrain axial motion of the pipe. A third cantilever supported the vertical branch of the system. In this case, a teflon sleeve was located between the pipe and the u-bolt, and the u-bolt was tightened such that it was only in light contact with the teflon sleeve. This configuration allowed vertical motion through the support. A picture of the cantilever configuration is presented in Figure 2. Material properties for the system are included in Table 1.

Table 1. 2-in. Schedule Type 304 Stainless Steel Pipe Properties [8]

Outer Diameter (OD)	60.3	mm
Inner Diameter (ID)	52.5	mm
Thickness (t)	3.91	mm
Mean Radius (R)	28.2	mm
Pipe Yourng's Modulus (E)	1.95×10^{11}	Pa
Pipe Mass Density (ρ)	8040	kg/m^3
Pipe Poisson's Ratio (ν)	0.31	
Hoop Frequency ($f_{breathing}$)	29	kHz
Flexural Frequency ($F_{flexural}$)	3.1	kHz

The piping system was instrumented with bonded strain gages at selected locations to measure both the hoop and axial response of the pipe, and axial strains in two directions along the cantilever beams. The strain gages were wired in quarter-bridges with Vishay 2310B signal conditioners operated in the wide band mode (140 kHz, -3 dB point). Pressure was measured using Piezo-electric pressure transducers (PCB 113A) placed along the side of the pipe and in the flange at the end of the pipe. All of the pressure and strain data was recorded using a 14-bit transient digitizer with a 1 MHz sampling frequency.

Table 2. 30% H_2 70% N_2O Mixture Properties at Each State as Computed with the Shock and Detonation Toolbox [9]

Initial Conditions		
Pressure	100	kPa
Temperature	295	K
Density	1.28	kg/m^3
CJ State		
Wave Speed (U_{CJ})	2088	m/s
Pressure (P_{CJ})	2.63	MPa
Temperature (T_{CJ})	3383	K
Sound Speed (c_{CJ})	1142	m/s
Post-Expansion State		
Pressure (P_{CJ})	0.958	MPa
Temperature (T_3)	3005	K
Sound Speed (c_3)	1107	m/s
Reflected Shock		
Pressure	6.53	MPa

See Note 1 under Acknowledgements

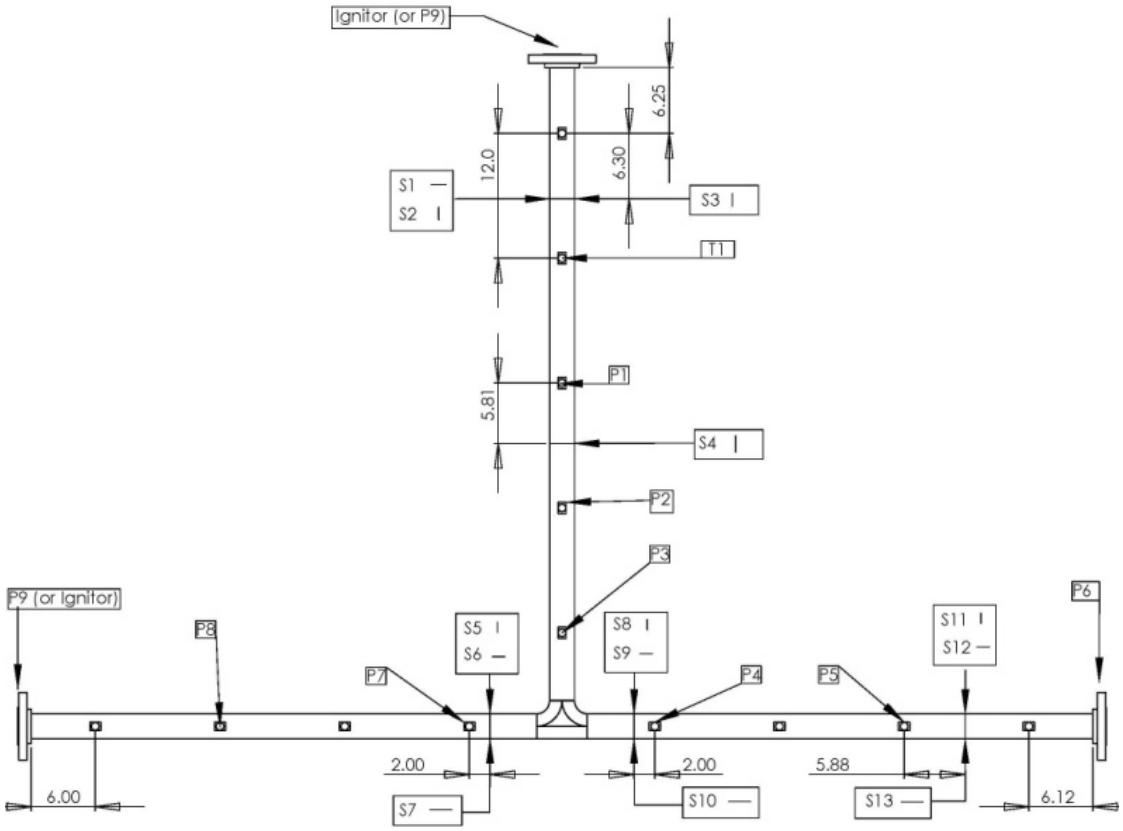

Figure 1. Experimental Setup with Sensor Locations

Figure 2. Photo of Cantilever Beam Support

Before each experiment, the piping system was evacuated to 40 mTorr and then filled with the test mixture of 30% hydrogen and 70% nitrous oxide using the partial pressure method. Once the pipe had reached 1 atm, the mixture was circulated through the system using a bellows pump connected to each end. The pump was run until the volume of the system has been circulated at least 5 times. Once the valves were closed to the circulation loop, the mixture was ignited using an ordinary spark plug located at the horizontal end of the pipe. In order to achieve rapid initiation of detonations, a short (305 mm) Shchelkin spiral was inserted into the beginning of the horizontal section to increase turbulence generation, which promotes flame acceleration and transition to detonation. The gas properties for 30 H_2 and 70 N_2O detonations are included in Table 2. The mixtures were chosen to be representative of potential hazards. These mixtures have detonation cell widths of about 3.3 mm, much smaller than the piping diameter, which results in a nearly ideal detonation wave that has a nearly planar front and propagates at wave speeds close to the Chapman-Jouguet value.

Experimental Results

A total of 15 shots were carried out including replicate shots to show test-to-test repeatability and shots using slightly different pipe configurations. In this paper we focus primarily on the data from Shots 43 and 44 (note the shot numbering includes prior tests using a different piping configuration). In Shot 43, the gas mixture was ignited at the top of the vertical leg, resulting in the detonation entering the tee from the branch. The spark plug was moved to the left (East) end of the system (see Figure 1) for Shot 44. In this configuration, the detonation enters the tee through the run. The expectation was that the detonation loads in the tee would differ depending on the direction from which the detonation enters the tee.

See Note 1 under Acknowledgements

Shot 43 Results

The purpose of Shot 43 was to study the system response from a detonation entering the tee through the branch. The gas mixture was ignited at the top of the vertical section and the resulting pressure and strain data are shown in Figure 3, Figure 4, and Figure 5. Shot 43 produced a near ideal detonation. The detonation velocity, determined from the detonation arrival time at each pressure transducer, was found to be within 1% of the values reported in Table 2, and the measured peak detonation pressures were consistent with the CJ detonation pressure. Peak reflection pressures of approximately 2.5 times the CJ detonation pressure were measured at P6 and P9.

As indicated in Figure 1, S1, S5, S8, and S11 measure hoop strain in the pipe and S2, S3, S4, S6, S7, S9, S10, S12, and S13 measure axial strain in the pipe. Peak hoop strains averaged 210 μstrain, which is consistent with a dynamic load factor (DLF) of 2 applied to the CJ detonation pressure using a single degree of freedom harmonic oscillator to model the radial response of the pipe.

Peak axial strains in the straight pipe ranged from approximately 115 to 200 μstrain, where the highest axial strains were measured near the tee. Unlike the hoop response, the axial response of the pipe is not dominated by a single mode. Rather, multiple modes contribute to the axial response including localized through-wall bending modes, uniaxial extensional modes, and macro pipe bending modes. These modes were discussed with respect to detonation loads at a bend by Ligon, et al. [4].

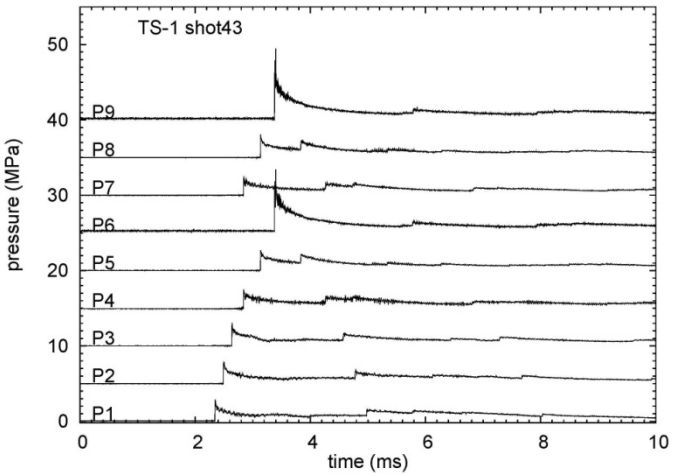

Figure 3. Shot 43 Pressure Measurements

Support strains are shown in Figure 5. These strain gages measure the loads on the two cantilever beams that are connected to the horizontal pipes. S25 and S26 measure the vertical/lateral loads and S24 and S27 measure the axial (relative to the pipe) loads. Due to the symmetric nature of the system and the loading, the lateral support strains are nearly identical and the axial support strains are approximately equal but 180º out of phase. The axial support loads appear to respond at a single characteristic frequency of approximately 450 Hz. This frequency compares favorably to a symmetric coupled extensional/bending mode of the system. This mode is excited when the detonation simultaneously reflects off the two blind flanges on either end of the horizontal run.

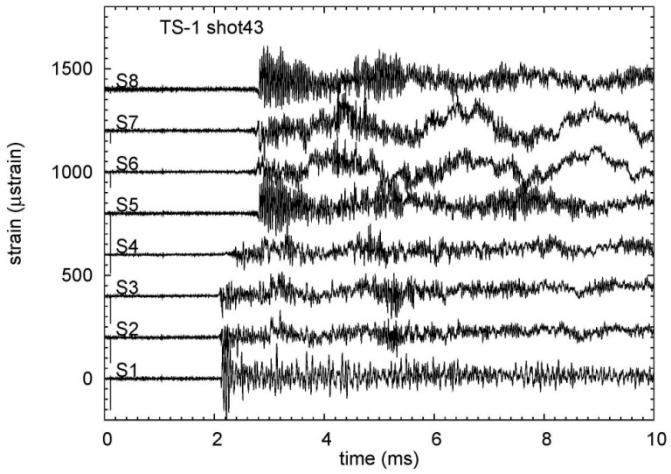

Figure 4. Shot 43 Pipe Strain Measurements

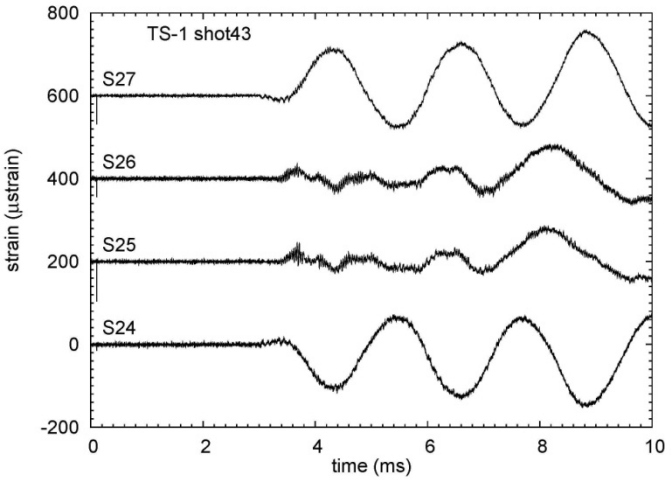

Figure 5. Shot 43 Support Strain Measurement

Shot 44 Results

Shot 44 was designed to investigate the response from a detonation entering the tee through the run. For this test, the spark plug was placed on the left end of the horizontal leg and pressure transducer P9 was moved to the top of the vertical leg (see Figure 1). A nearly ideal detonation was produced and the strain data are shown in Figure 6 and Figure 7.

Overall, Shot 44 strains are lower than Shot 43 strains. The largest reductions occurred near the tee, particularly the axial strains at S6, S7, S9, and S10. On average, these strains are approximately 20% lower than in Shot 43 when the detonation entered the tee from the branch. Similarly, measured vertical support strains decreased by approximately 10%. These results suggest that the load at the tee does depend on the direction from which the detonation enters.

See Note 1 under Acknowledgements

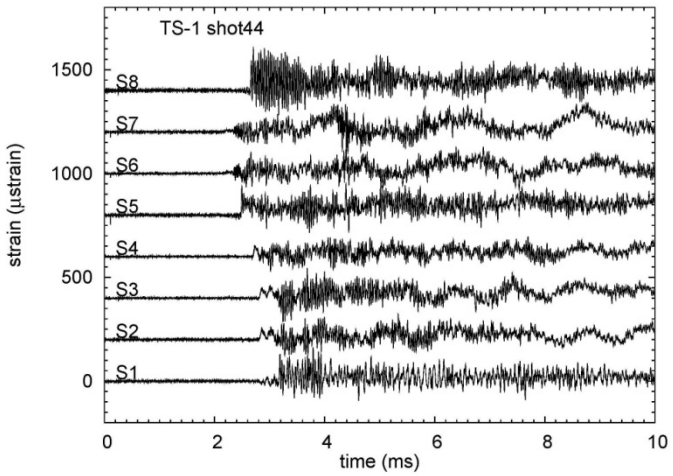

Figure 6. Shot 44 Pipe Strain Measurements

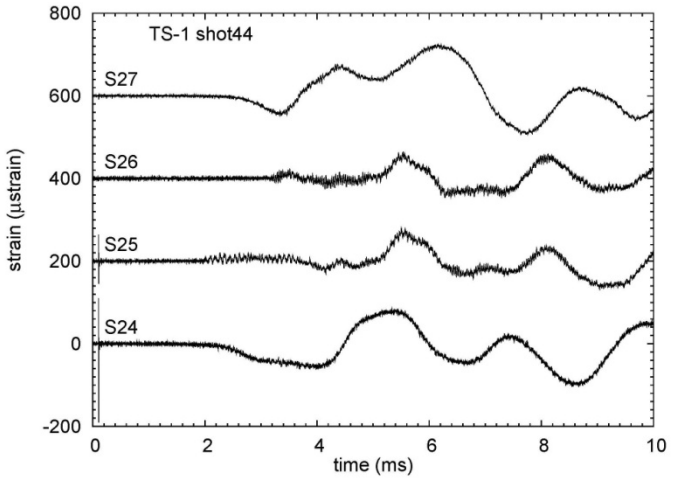

Figure 7. Shot 44 Support Strain Measurement

Detonation Modeling

Detonations are characterized by a jump from the initial pressure to the peak detonation pressure followed by approximately exponential pressure decay. When the gas mixture detonates, the reaction products are highly compressed and the pressure decays as the gasses expand behind the detonation front. In confined detonations, the pressure in the expansion fan behind the detonation front plateaus to a *post-expansion* pressure P_3 that is still well above the initial pressure. The Taylor-Zel'dovich (TZ) detonation solution describes the pressure variation between the peak CJ pressure and the post-expansion pressure. The solution for the spatial and temporal distribution of pressure throughout the pipe is given by Equation (1) below [9],[10]. The subscripts indicate states at which each parameter is evaluated. The subscript 1 indicates the initial state prior to the arrival of the detonation, 2 is the CJ state, and 3 is the post-expansion state. The quantities P_3 and c_3 are the pressure and speed of sound in the post-expansion region

$$P_{det}(x,t)=\begin{cases} P_1 & U_{CJ}<x/t<\infty \\ P_3\left[1-\dfrac{\gamma_2-1}{\gamma_2+1}\left(1-\dfrac{x}{c_3 t}\right)\right]^{\frac{2\gamma_2}{\gamma_2-1}} & c_3<x/t<U_{CJ} \\ P_3 & 0<x/t<c_3 \end{cases} \quad (1)$$

$$c_3=\frac{\gamma_2+1}{2}c_{CJ}-\frac{\gamma_2-1}{2}U_{CJ} \quad (2)$$

$$P_3=P_{CJ}\left(\frac{c_3}{c_{CJ}}\right)^{\frac{2\gamma_2}{\gamma_2-1}} \quad (3)$$

The ratio of specific heats γ_2, speed of sound at the CJ state c_3, and the detonation velocity U_{CJ} can be calculated using chemical equilibrium software, such as CEA [11] or the Shock and Detonation Toolbox [9].

Reflected Detonation Model

At the ends of the system, the detonation reflects off the blind flanges and a reflected shock propagates back into the pipe. An empirical model for the reflected detonation was developed based on the measured reflected detonation pressure. The pressure behind the reflected shock uniformly decays as the gases expand away from the flange until the gas reaches the post-expansion pressure P_3. The pressure behind the shock was represented by the double exponential shown in Equation (4). The motivation for using the double exponential was to accurately capture both the rapid decay from the 2.5xP_{CJ} peak reflected pressure [12], calculated using the Shock and Detonation Toolbox [9], and the longer term decay to the post-expansion pressure. The time constants T_1 and T_2 were adjusted to fit the measured pressure data at P6 and their final values were 540 μs and 90 μs, respectively. The fitted pressure time-history is compared to the P6 pressure data from Shot 43 in Figure 8. The reflected shock velocity U_{ref}, was assumed to be equal to the post-expansion sonic velocity (c_3).

$$\mathrm{P_{ref}}(x,t)=\begin{cases} P_{det}(x,t) & U_{ref}<\dfrac{x}{t}<\infty \\ \left(2.5P_{CJ}-P_3\right)\dfrac{\left(e^{-t/T_1}+e^{-t/T_2}\right)}{2}+P_3 & 0<\dfrac{x}{t}<U_{ref} \end{cases} \quad (4)$$

The expression in Equation (4) is an empirical model that is based on experimental observations of pressure and validated for the piping model and explosive gases used in the experiments. A more general approach is to consider the dynamics of the gases and the reflected shock wave that brings the flow to rest. These issues are discussed by Karnesky et al. [6], who provide a model that can be used for an arbitrary mixture and geometry.

See Note 1 under Acknowledgements

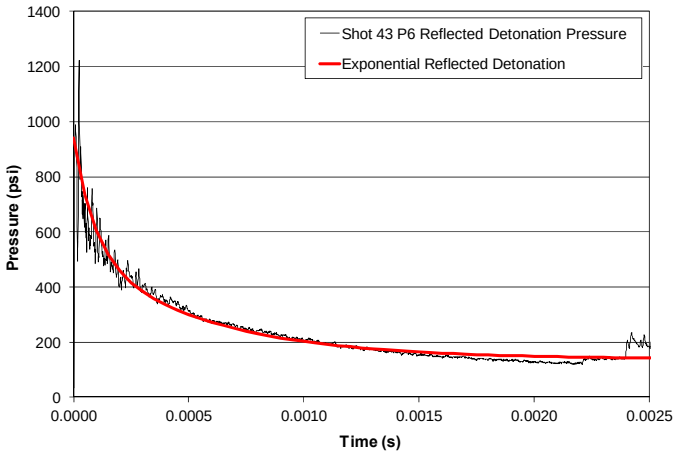

Figure 8. Shot 43 P6 Pressure Compared to the Reflected Detonation Model

Tee Detonation Models

A detonation can enter a tee through the branch or either leg of the run. When a detonation enters through the run (see Figure 9), the effect on the detonation will depend on the relative magnitude of the cell width and the pipe diameter. For sufficiently small cell widths compared to the diameter, the case in the present study, the wave propagating along the run is not expected to experience significant perturbations. The detonation front expands as it diffracts around the edge of the transition to the branch connection, but the momentum of the reaction products in the expansion fan behind the front can pass through the run of the tee without interference. Small reflections may occur, such as at the branch transition shown in Figure 9, but these localized reflections are not expected to achieve high pressures.

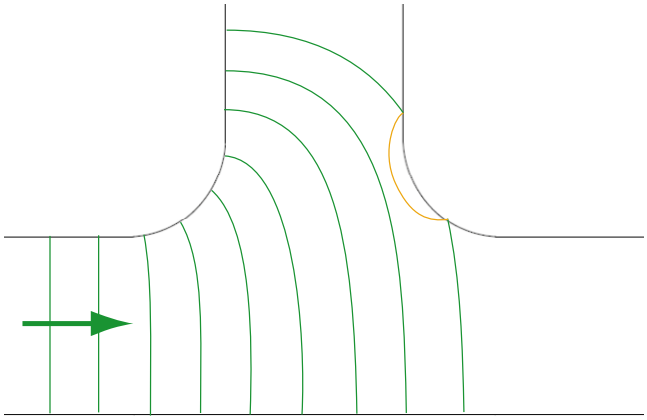

Figure 9. Detonation Entering Tee through the Run

When the detonation enters through the branch, however, the detonation front again expands as it diffracts around the branch transition. The expansion may result in a portion of the wave slowing down and the shock front partially decoupling from the reaction zone. The shock or detonation will continue to propagate towards the opposite wall of the tee (see Figure 10). When the shock or detonation wave reflects from the wall, the momentum of the gas behind the front is turned, and this change in direction is expected to generate high pressures over a relatively large surface area. The reflection of the shock front will increase the temperature and pressure, re-initiating the coupling between the shock and reaction front so that a detonation continues up through the branch.

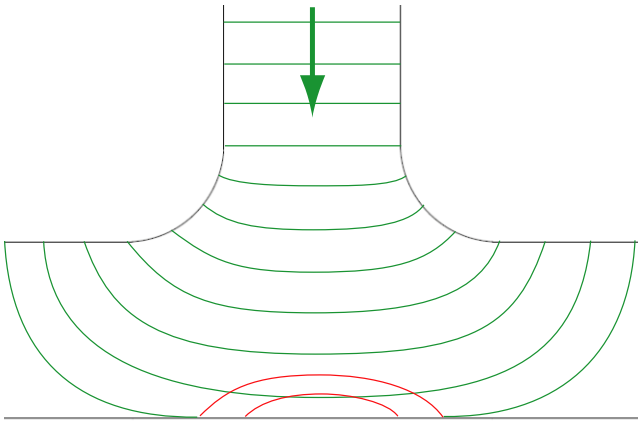

Figure 10. Detonation Entering Tee through the Branch

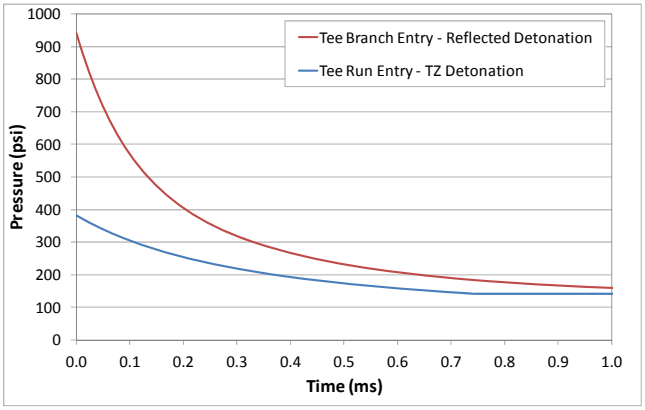

Figure 11. Tee Pressure Time-Histories

Both of these events are simplified for the purpose of the analyses presented in this paper. For a detonation entering through the run, the detonation is assumed to propagate through the tee without any disturbance, and the TZ detonation equations, discussed above, are applied to all surfaces within the tee. For a detonation entering through the branch, the detonation pressure on the opposite wall of the tee is modeled using the reflected detonation model described by Equation (4). Any reflected shock waves that may be produced during the event are assumed to attenuate quickly and are neglected. Thus, the only region of the wall that is loaded with the increased pressure is the area that is within the projected area of the branch line (see Figure 14). These two pressure time-histories are plotted in Figure 11.

See Note 1 under Acknowledgements

Finite-Element Modeling

The finite-element (FE) model of the system geometry was constructed in ANSYS using 8-node shell elements (SHELL93). Eight elements, with an aspect ratio of approximately 2:1, were used to describe the circumference of the pipe. The work by Tang was used as the basis for the axial element length (12.7 mm) [13]. Tang presents a solution for a pressure wave in a pipe propagating at a constant velocity. The wave equations described by Tang were used to calculate a wavelength (73.66 mm) of the excited flexural mode. The model was constructed such that nodes were placed at the same locations as the strain gages in the experiments.

The apparatus is supported on cantilever beams with U-bolts coupling the beam to the pipe. The U-bolt connection to the pipe is modeled by creating a pilot node at the center of the shell elements that is connected to the shells using a "spider-web" of radially-oriented beam elements. The "spider-web" beams were given a large area and second moment of area (bending moment). These beam element properties couple the beam and shell element degrees of freedom, and restrict the shells from dilating radially ("breathing") to model the contact with the U-bolt.

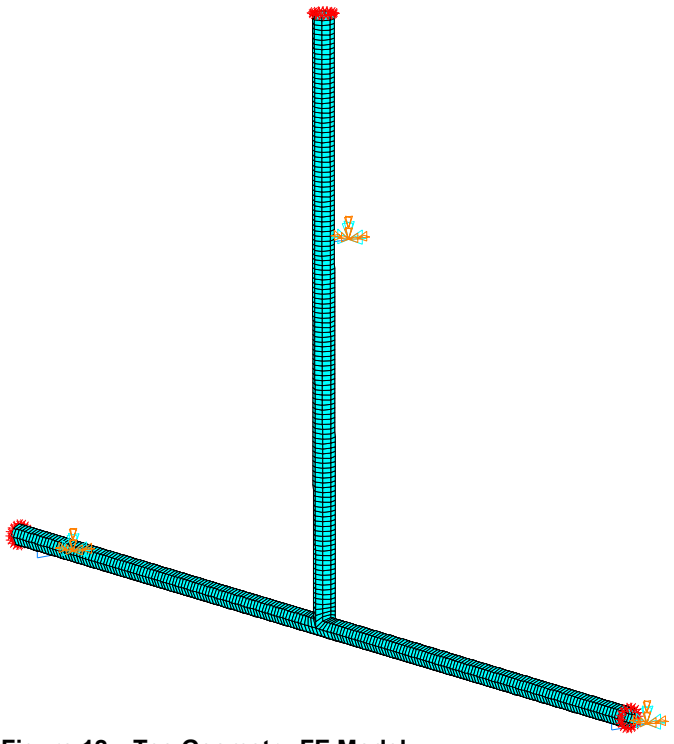

Figure 12. Tee Geometry FE Model

The cantilever beam was modeled using beam elements that were offset from the center of the pipe using an additional rigid beam element. The rigid beam connects the end of the cantilever beam elements to the shell element pilot node. The pilot node was coupled to the rigid beam element node in the appropriate translational degrees of freedom (all three directions for the U-bolts on the horzintal leg, and only in the lateral directions for the U-bolt on the branch). The far end of the cantilever was fixed in all six directions. The full finite-element model and a detail view of the cantilever beam supports are shown in Figure 12 and Figure 13, respectively.

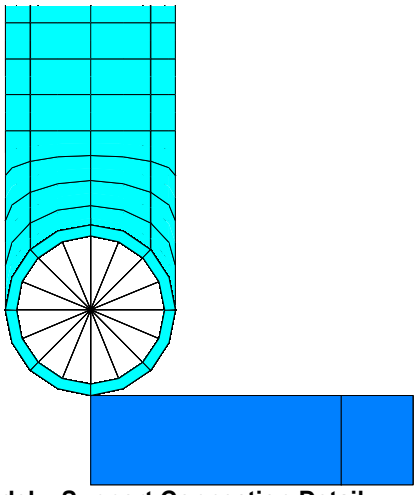

Figure 13. FE Model – Support Connection Detail

The implicit time integration analysis used a time step equal to 1/20 the breathing mode period, calculated using Equation (5) [14], and the analysis simulated 15 ms of response. No damping was assumed, due in part to the limitations of Rayleigh damping where damping can only be specified at two frequencies.

$$f_{breathing} = \frac{1}{2\pi R}\sqrt{\frac{E}{\rho(1-\nu^2)}} \tag{5}$$

At each time step the appropriate detonation pressure is applied to the inner surface of the shell elements, depending on their location in the pipe. In straight pipe, the forward propagating detonation pressure was calculated using Equation (1), and the reflected detonation pressures, applied to elements behind a reflected shocks, were calculated using Equation (4). As described above, the pressure behind the reflected shock is approximately uniform and all elements behind the reflected shock were loaded with the same decaying pressure.

When the detonation enters the tee, Equation (1) is applied everywhere except when it enters through the branch. In the branch case, a separate reflected detonation pressure time-history (Equation (4)) is applied to the elements within the projected area of the branch line (see Figure 14). The tee reflected detonation time constant T_2 is taken to be the same as the value fitted to the P_6 pressure time-history shown above (90 μs), but the T_1 time constant from the fit is reduced by the ratio of the distance from ignition to the tee over the distance to the end of the system (0.56). This ratio was applied to account for the detonation expansion wave lengthening with increasing propagation distance.

See Note 1 under Acknowledgements

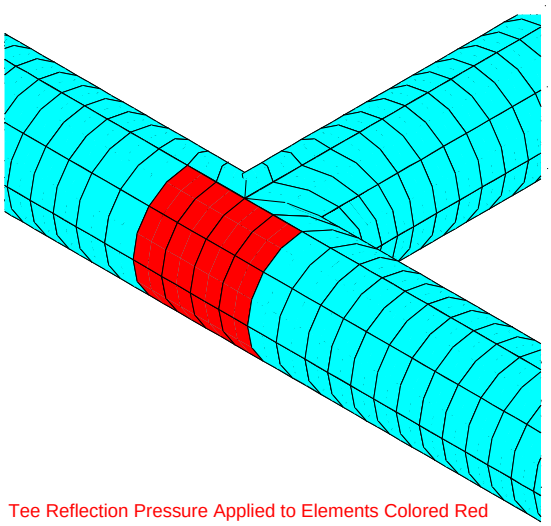

Figure 14. Tee Reflection Pressure Elements

Finite-Element Results

The FE results of interest are the pipe and support strains at the locations indicated in Figure 1. The results are compared on a one-to-one basis with the measured strain results in a number of figures that are discussed in the following sections. It is noted that the FE strain results shown in these figures are shifted forward in time by 1.94 ms to line up with the measured strain data. This time shift represents the difference in the reference time for the start of the computation and the experiment.

Low-pass filtered axial strains are also presented. The axial strains were filtered by applying a forward moving average over a 50μs window. Filtering removes the high-frequency component in the axial strain response to highlight the lower frequency extensional and bending modes. The high-frequency component, discussed in detail by Ligon et al. [4], is a result of the flexural mode that is excited by the detonation. The flexural mode shape induces through-wall bending of the pipe wall, in additional to axial Poisson coupling with the hoop response. Although these stresses may impact the fatigue life of the pipe, they obscure the components of the axial response that are due to the detonation forces generated at the tee and closed-ends of the system.

In addition to the response due to the pressure transient, heat transfer from the reaction products heat up the pipe causing thermal expansion. The impact of thermal expansion on the measured strains is readily observed after filtering. Thermal strains are evident in the filtered hoop strains shown in Figure 15. At 4 ms, the average strain is approximately 30 μs, which is consistent with the expected hoop strain due to an internal pressure equal to P_3. After this time, the average strain increases due to thermal expansion. Thermal strains become significant after approximately 6 ms. Therefore, maximum pipe strains are only reported for 0-6 ms. Support strains are reported for the entire duration of the FE analysis.

Detonation Entering through the Run

Results from the FE analysis of a detonation entering the tee through the run are compared to the strain data from Shot 44. Selected pipe strain traces are shown in Figure 16 through Figure 22 and maximums are tabulated in Table 3. As shown in Figure 16, hoop strains show reasonable correlation in the early response.

Axial strains, both filtered and unfiltered, are shown in Figure 17 through Figure 22. The early response at S2 is a result of the initial unbalanced load at the tee. When the detonation propagates through the tee, the unbalanced load produces a uniaxial tension wave that propagates up the branch line. The tension wave is observed before the high-frequency response. As discussed by Ligon et al. [4], the tension wave travels faster than the detonation. The remainder of the response compares favorably until approximately 6 ms. The high-frequency component of the axial response is generally under-predicted.

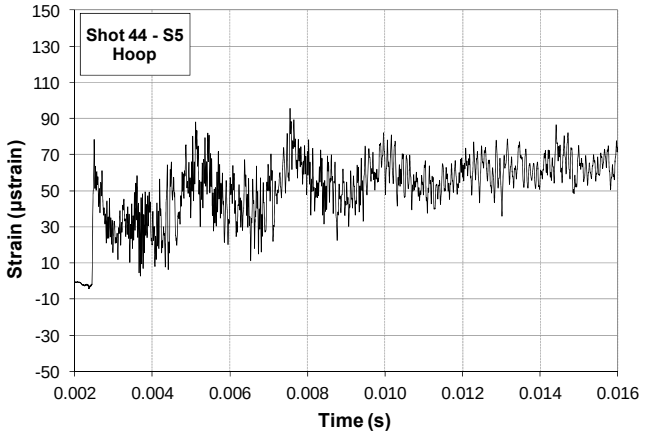

Figure 15. Filtered Hoop Strains Showing Thermal Strain

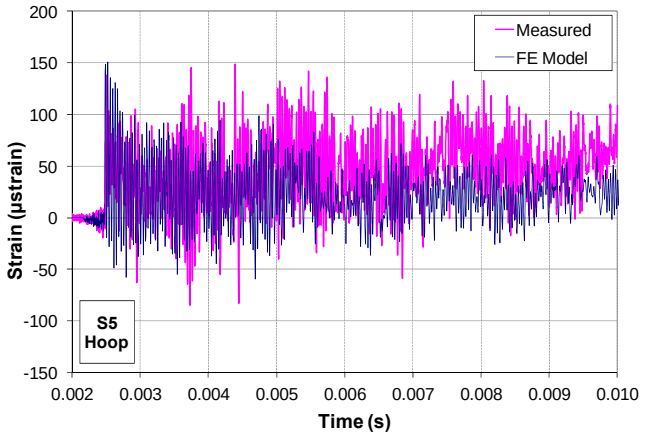

Figure 16. Comparison of FE Results to Shot 44 Data at S5

See Note 1 under Acknowledgements

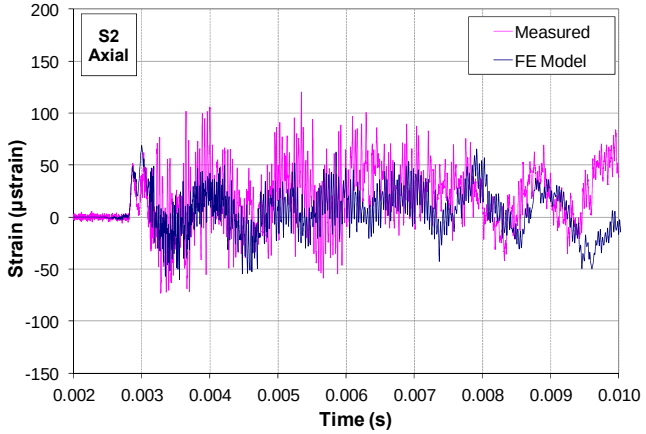

Figure 17. FE Results and Shot 44 Data at S2

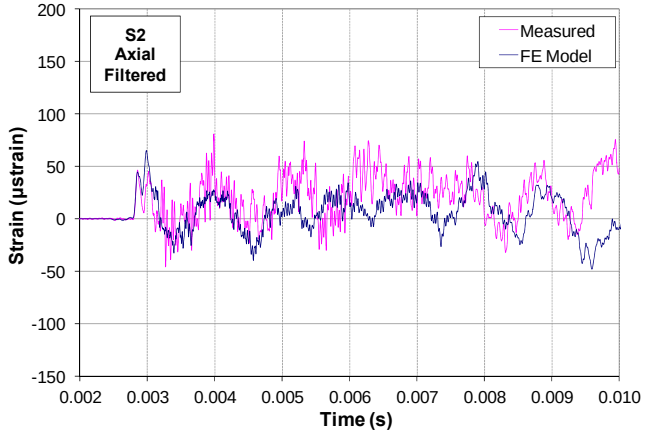

Figure 18. Filtered FE Results and Shot 44 Data at S2

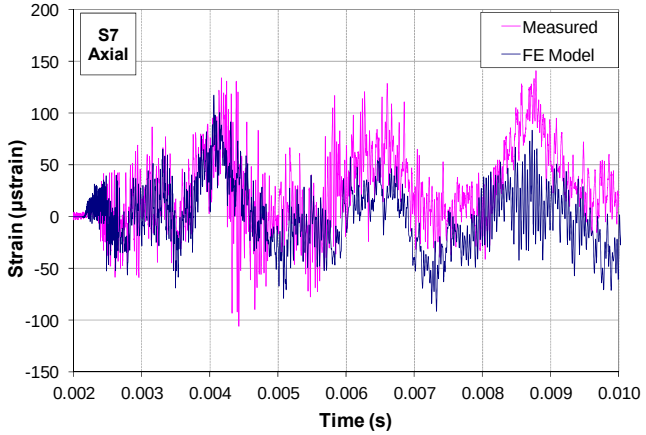

Figure 19. FE Results and Shot 44 Data at S7

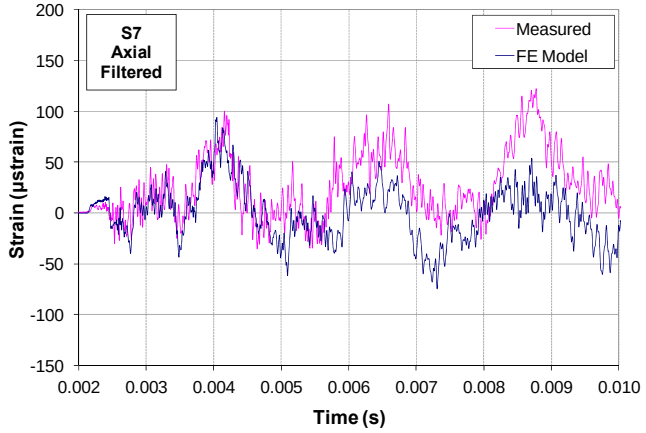

Figure 20. Filtered FE Results and Shot 44 Data at S7

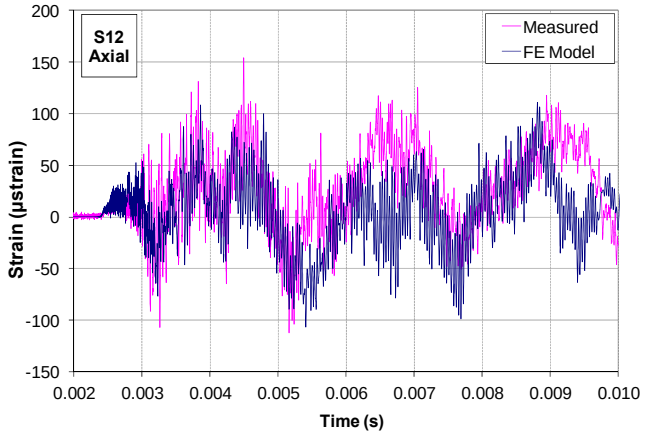

Figure 21. FE Results and Shot 44 Data at S12

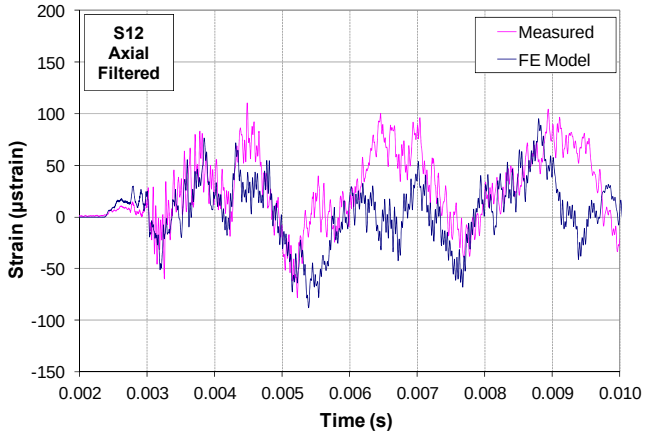

Figure 22. Filtered FE Results and Shot 44 Data at S12

Strain results at S7 and S12 are also in agreement with the measured strains. In both cases, the first significant excursion is accurately predicted. At S7, the predicted response continues to correlate with the data until approximately 5 ms. At S12, the peak at approximately 4.5 ms is under-predicted. The high-frequency components are more consistent with the data compared to at S2.

Support strains, shown in Figure 23 through Figure 25, are over-predicted by the FE model. The most significant over-prediction is in the axial (with respect to the pipe) direction. The early response is comparable, but the model overshoots the peaks by 35% to 60%. In the lateral direction (parallel to the branch line), the predicted strains contain higher frequencies than were observed in the experiments, but the peaks are only slightly over-predicted.

See Note 1 under Acknowledgements

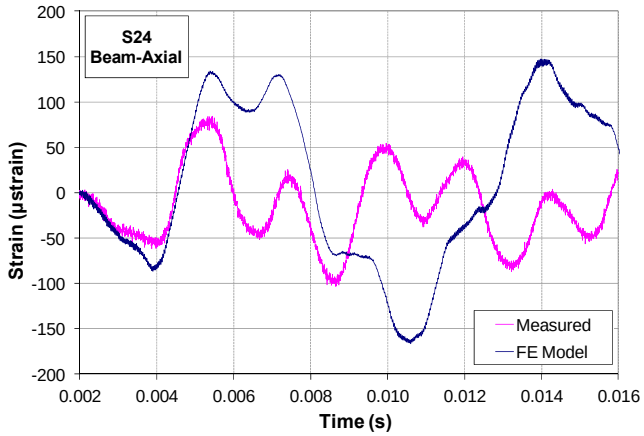

Figure 23. FE Results and Shot 44 Data at S24

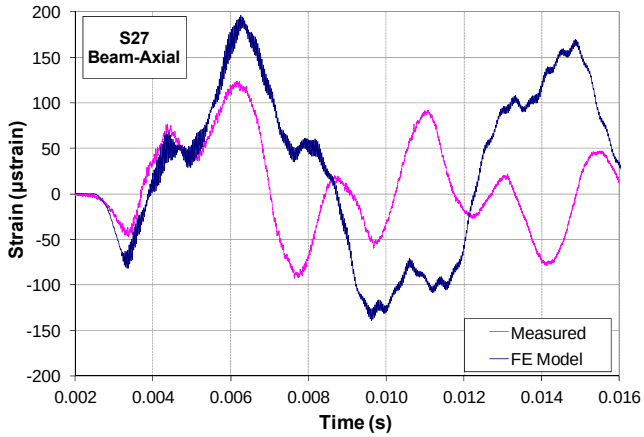

Figure 24. FE Results and Shot 44 Data at S27

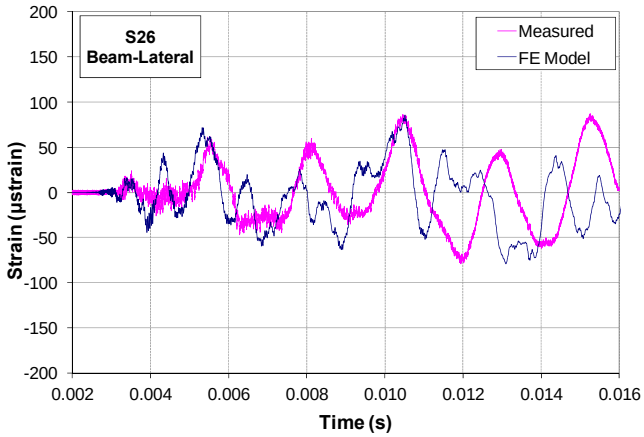

Figure 25. FE Results and Shot 44 Data at S26

Maximum strains are tabulated in Table 3 and presented visually in Figure 26. Figure 26 shows that there is a reasonable amount of scatter (±30%) in the ability of the model to predict maximum strains. On average pipe strains are under-predicted and support strains are over-predicted. Overall, these results support the conclusion that a detonation is not significantly perturbed when it enters a tee through the run. Stated alternatively, the detonation pressure is not significantly amplified when a detonation enters through the run of the tee.

Table 3. Maximum Strains

	Branch Entry			Run Entry		
Gage	Shot 43	FEA	% Diff.	Shot 44	FEA	% Diff.
Filtered Axial Strains (µstrain)						
S2	90	89	-1%	81	65	-19%
S3	76	89	18%	82	67	-18%
S4	102	98	-3%	63	75	19%
S6	108	101	-7%	86	72	-16%
S7	135	100	-26%	100	94	-6%
S9	99	101	2%	94	72	-24%
S10	135	100	-26%	95	78	-18%
S12	97	132	35%	110	77	-31%
S13	107	78	-27%	70	93	32%
Hoop Strains (µstrain)						
S1	264	138	-48%	163	175	7%
S5	222	160	-28%	149	151	1%
S8	210	161	-24%	208	175	-16%
S11	144	185	28%	145	171	18%
Cantilever Strains (µstrain)						
S24	73	87	19%	110	147	34%
S25	94	121	29%	87	103	18%
S26	104	117	13%	88	91	4%
S27	157	114	-27%	124	197	59%

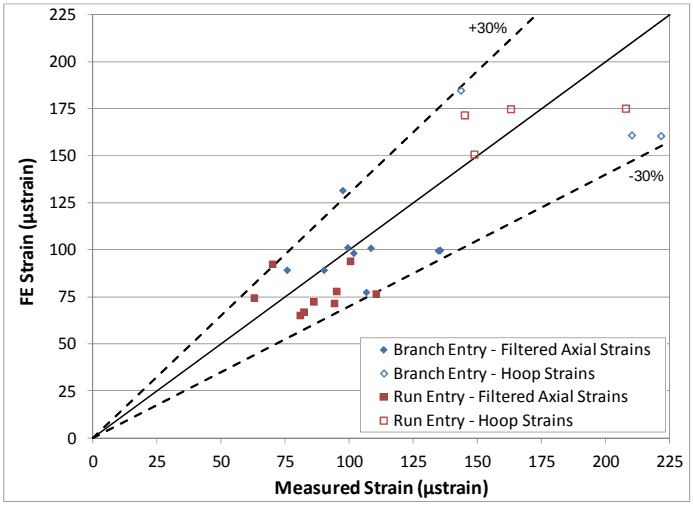

Figure 26. Maximum Pipe Strains

Detonation Entering through the Branch

The results from the analysis of a detonation entering through the branch are compared to selected strain data from Shot 43 in Figure 27 through Figure 33. On average, hoop strains are under-predicted, notably near the tee. The under-prediction is potentially due to reflections that occur within the tee itself. Axial strains are generally in better agreement with the measured strains. Although some small differences exist, the frequency and magnitude of the predicted axial strains are consistent with the data for the entire 10 ms duration shown in the figures.

See Note 1 under Acknowledgements

When the detonation pressurizes the tee, a tension wave is sent up the branch leg of the system. This tension wave is evident and well predicted at S3. After the tension wave passes, the model appears to exhibit less damping than is observed in the measured strains. Excellent correlation is observed between the results and measured strains at S9 and S13. The model does not deviate significantly from the measured response until the peak at approximately 9 ms.

Predicted support strains also compare favorably with the data from Shot 43. At first, the predicted axial support loads shown in Figure 34 are in agreement with the measured strains, but as time continues, the predicted frequency of the response is slightly higher. This suggests that there is additional mass in the system that is not included in the model, which may be due to the neglected mass of the instrumentation. The measured axial loads maximize after two cycles, but the model predicts the response to slowly decay, leading to under-prediction of the maximum load. Lateral loads, shown in Figure 35, are again predicted to contain higher frequency components that were not measured in the experiments. The maximum lateral loads, however, are over-predicted.

In conclusion, applying an amplified pressure within the tee produced results that were in general agreement with the measured strains. In this analysis, the amplified pressure was assumed to be comparable to a reflected detonation and was only applied over a limited surface area. Measured hoop strains near the tee suggest that the amplified pressures may exist over a larger area.

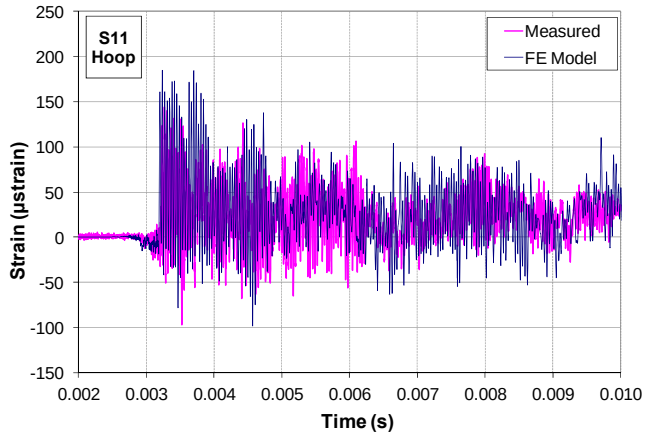

Figure 27. FE Results and Shot 43 Data at S11

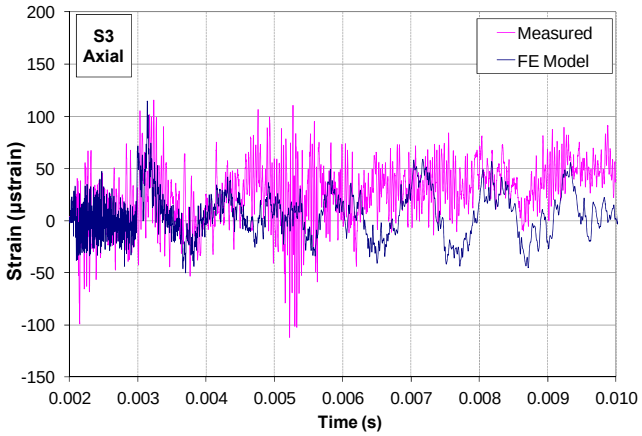

Figure 28. FE Results and Shot 43 Data at S3

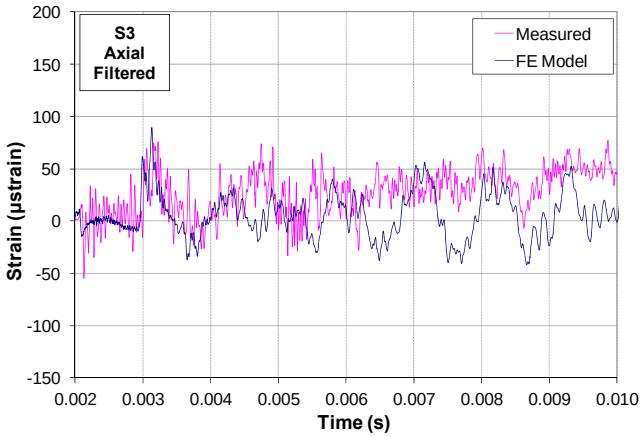

Figure 29. Filtered FE Results and Shot 43 Data at S3

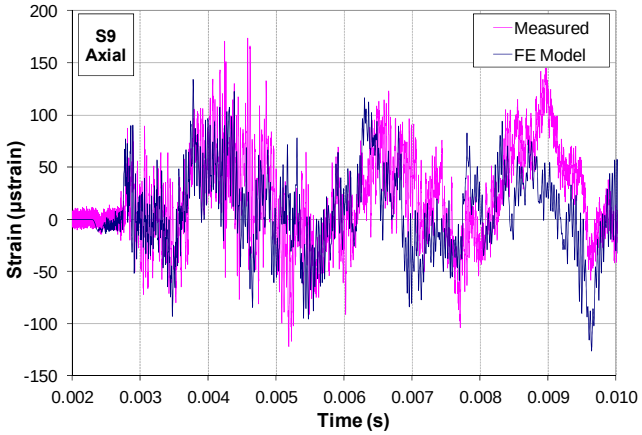

Figure 30. FE Results and Shot 43 Data at S9

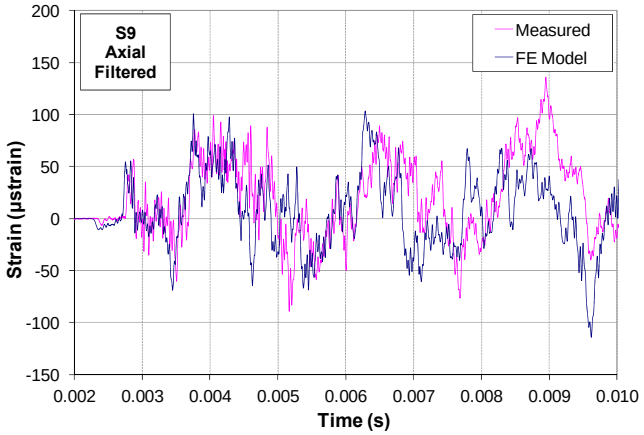

Figure 31. Filtered FE Results and Shot 43 Data at S9

See Note 1 under Acknowledgements

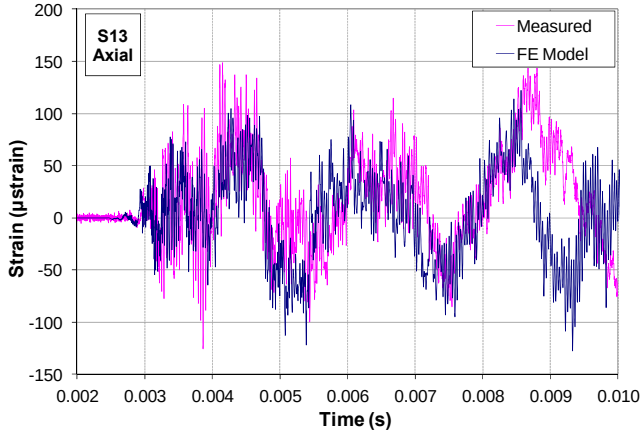

Figure 32. FE Results and Shot 43 Data at S13

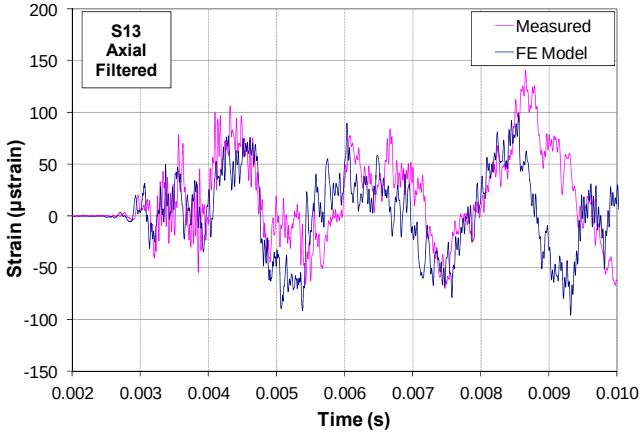

Figure 33. Filtered FE Results and Shot 43 Data at S13

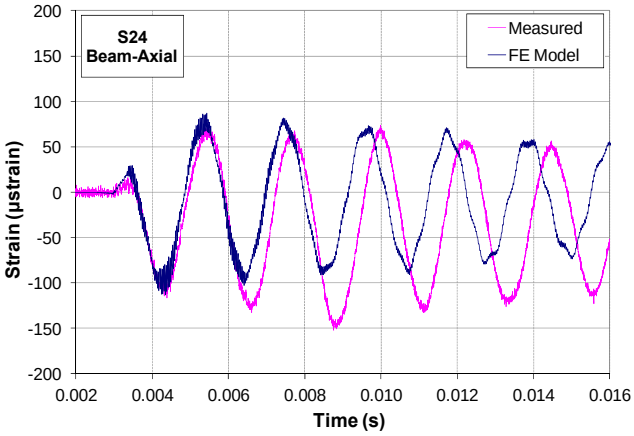

Figure 34. FE Results and Shot 43 Data at S24

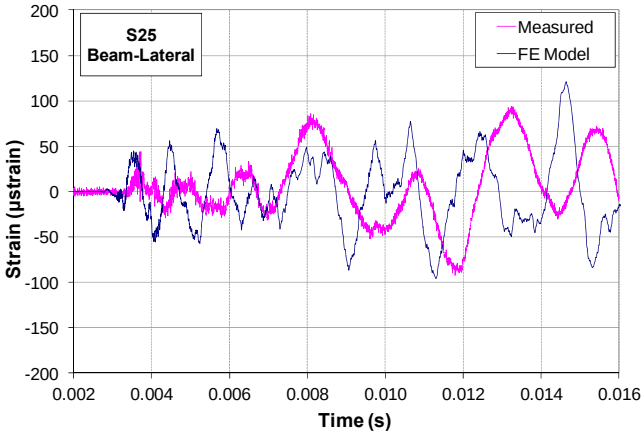

Figure 35. FE Results to Shot 43 Data at S25

CONCLUSIONS

An unbalanced force is generated when a detonation propagates through a tee. The work described in this paper has shown that the magnitude of this force depends on the direction from which the detonation enters the tee. When the detonation enters through the run, the detonation pressure can be modeled assuming no perturbation. A detonation entering through the branch, however, encounters an abrupt change in direction that results in amplified pressures due to the change in momentum of the gas behind the detonation front.

In this work, the amplified pressures were modeled as a reflected detonation. Although a reflected detonation reaches a pressure that is approximately 2.5 times higher than the detonation pressure, the response of the piping is also related to the impulse (integrated pressure) associated with the pressure time-history. Depending on the chosen integration limit, the impulse associated with the reflected detonation ranges from 1.6 to 2.1 times greater than a TZ detonation. Therefore, it is concluded that when the detonation enters through the branch the detonation load at the tee increases by approximately a factor of 2.

FE simulations using these detonation pressure time-history models produced satisfactory results compared to measured strain data. This work did not focus on the strains in the tee itself, and more sophisticated models may be required to appropriately model the local response.

ACKNOWLEDGEMENTS

We acknowledge the very substantial contributions of Dr. Raza Akbar in designing the TS-1 specimen as well as constructing and operating the test facility at Caltech. The work described in this paper was performed in support of the U.S. Department of Energy's (DOE's) Hanford Tank Waste Treatment and Immobilization Plant (WTP) Project (contract number DE-AC27-01RV14136), under subcontract to DOE prime contractor Bechtel National, Inc.

See Note 1 under Acknowledgements

REFERENCES

[1] Ciccarelli, G., and Dorofeev, S., 2008, "Flame acceleration and transition to detonation in ducts," Progress in Energy and Combustion Science, 34(4), pp. 499-550.

[2] Lee, J. H. S., 2008, The Detonation Phenomenon, Cambridge University Press. New York, NY.

[3] Shepherd, J. E., 2009, "Structural Response of Piping to Internal Detonation," Journal of Pressure Vessel Technology, 131(3), pp. 031204.031201-031204.031213.

[4] Ligon, T C., J., Shepherd, J. E., and Gross, D. J., 2011, "Forces on Piping Bends Due to Propagating Detonations," ASME, PVP-Vol. 5, PVP2011-57278.

[5] Beltman, W. M., and Shepherd, J. E., 2002, "Linear elastic response of tubes to internal detonation loading.," Journal of Sound and Vibration, 252(4), pp. 617-655.

[6] Karnesky, J., Damazo, J., Shepherd, J. E., and Rusinek, A., 2010, "Plastic Response of Thin-Walled Tubes to Detonation," ASME. PVP-Vol. 4, PVP2010-25749.

[7] Shepherd, J. E., and Akbar, R., 2010, "Piping System Response to Detonations. ES1, TS1, and SS1 testing." GALCIT Report FM2009.001, Pasadena, CA.

[8] 2010, Boiler and Pressure Vessel Code, Section II, "Materials," Part D – Properties (Customary), The American Society of Mechanical Engineers. New York, NY.

[9] Brown, S., Zeigler, J., and Shepherd, J. E., 2008, "Numerical Solution Methods for Shock and Detonation Jump Conditions," Technical Report No. FM2006.006, Graduate Aeronautical Laboratories - California Institute of Technology, Pasadena, CA.

[10] Zel'dovich, Y. B., and Kompaneets, A. S., 1960. "Theory of Detonation." Academic Press, NY. English translation of original Russian.

[11] Gordon, S., and McBride, B., 1994, "Compute Program for Calculation of Complex Chemical Equilibrium Compositions and Applications," Reference Publication No. RP-1311, NASA.

[12] Shepherd, J. E., Teodorcyzk, A., Knystautas, R., and Lee, J. H. S., "Shock Waves produced by Reflected Detonations," Proc. Progress in Astronautics and Aeronautics, AIAA, pp. 244-264.

[13] Tang, S., 1965, "Dynamic Response of a Tube under Moving Pressure." Journal of Engineering Mechanics Division. Proceedings of the American Society of Civil Engineers, Vol. 91.

[14] Blevins, R. D., 1979, Formulas for Natural Frequency and Mode Shape, Kreiger Publishing Company, Malabar, FL.

See Note 1 under Acknowledgements